Teng, G., and Baker, J. W. (2020). "Short-term probabilistic hazard assessment in regions of induced seismicity." *Bulletin of the Seismological Society of America*, 110(5), 2441-2453.

Short-term probabilistic hazard assessment in regions of induced seismicity

Ganyu Teng, Jack W. Baker

Abstract

This project introduces short-term hazard assessment frameworks for regions with induced seismicity. The short-term hazard is the hazard induced during the injection for hydraulic-fracturing-induced earthquakes. For wastewater-disposal-induced earthquakes, it is the hazard within a few days after an observed earthquake. In West Texas, hydraulic-fracturing-induced earthquakes cluster around the injection activities, and the earthquake occurrence varies greatly in time and space. We develop a method to estimate the hazard level at the production site during the injection, based on past injection and earthquake records. The results suggest that the injection volume has a negligible effect on short-term earthquake occurrence in this case, because injection volumes per well fall within a relatively narrow range, whereas the regional variations in seismic productivity of wells and b-values are important. The framework could be easily modified for implementation in other regions with hydraulic-fracturing-induced earthquakes. We then compare the framework with wastewater-disposal-induced earthquakes in Oklahoma-Kansas and natural earthquakes in California. We found that drivers of short-term seismic hazard differ for the three cases. In West Texas, clustered earthquakes dominate seismic hazards near production sites. However, for Oklahoma-Kansas and California, the short-term earthquake occurrence after an observed mainshock could be well described by the mainshock-aftershock sequence. For Stillwater in Oklahoma, aftershocks contribute less to the hazard than San Francisco in California, due to the high Poissonian mainshock rate. For the rate of exceeding a Modified Mercalli intensity of 3 within seven days after an M4 earthquake, the aftershock sequence from natural earthquakes contributed 85% of the hazard level, whereas the aftershock contribution was only 60% for induced earthquakes in Oklahoma. Though different models were implemented for hazard calculations in regions with hydraulic fracturing versus wastewater injection, injection activities could be drivers of short-term hazard in both cases.

Introduction

Probabilistic seismic hazard analysis typically ignores aftershock sequences and assumes a Poissonian seismic occurrence. Such assumptions are not valid when considering a short time range due to the presence of aftershock sequences. There have been various models developed to describe short-term earthquake occurrence based on natural earthquake catalogs. Most of them assumed an earthquake sequence consisting of Poissonian mainshocks followed by exponentially-decay aftershocks. Reasenberg and Jones (1989) combined the modified Omori's Law and the Gutenberg-Richter distribution of magnitudes to describe the aftershock sequences. Agnew and Jones (1991) considered foreshocks, background earthquakes, and characteristic earthquakes in their earthquake occurrence model and focused on the probability that the observed earthquake would be followed by a larger earthquake in a short time range. Michael (2012) compared these two models, and introduced a

generalized clustering model by modifying Reasenberg and Jones (1989) to include the characteristic seismic behaviors. In Gerstenberger *et al.* (2005), the seismic hazard consisted of the Poisson and the time-dependent hazard. The latter was computed using a clustering model that included 1) a generic-clustering model (Reasenberg and Jones, 1989), 2) a sequence-specific model that described the aftershocks from the ongoing earthquake sequence, and 3) a spatially heterogeneous model that considered the spatial difference in parameters. Page *et al.* (2016) extended Reasenberg and Jones (1989) by considering time-varying magnitude of completeness and the uncertainty in aftershock productivity. They developed regional aftershock parameters for tectonic regions in Garcia *et al.* (2012). The modified model (Reasenberg and Jones, 1989; Page *et al.*, 2016) has been implemented in the U.S. Geological Survey (USGS) aftershock forecast (Michael *et al.*, 2020). Field *et al.* (2017) uses Epidemic Type Aftershock Sequence (ETAS) together with UCERF3 to describe the time-dependent earthquake occurrence. However, the models mentioned above were mostly developed based on natural earthquake catalogs, and limited studies have been done for regions with induced seismicity. Michael *et al.* (2016) studied the aftershock sequence of the 2016 M5.8 Pawnee, Oklahoma, earthquake, and observed higher aftershock productivity compared to the generic model in Page *et al.* (2016). Such high aftershock productivity was also observed in Llenos and Michael (2013), where they modeled the change in earthquake rate in Oklahoma using the ETAS model. However, the existing mainshock and aftershock models were mostly developed for natural earthquakes or relatively large mainshocks. They may not be suitable for induced seismicity that involves human activities and more small earthquakes.

This project develops a short-term hazard assessment framework for regions of induced seismicity. In particular, we focus on earthquakes produced by hydraulic fracturing in West Texas, where the high-pressure injection of water results in fracking or induces slip on faults (Ellsworth, 2013; Frohlich *et al.*, 2016). West Texas has a long history of fracturing and has experienced induced earthquakes since the 1960s (Snee and Zoback, 2018). There have been studies to quantify the hazard level induced by hydraulic fracturing. Langenbruch and Zoback (2019) quantified the annual seismic rate induced by hydraulic fracturing in Oklahoma using a seismogenic index model. Ghofrani *et al.* (2019) introduced year-by-year probabilistic seismic hazard maps for the sedimentary basin in western Canada. Their models considered both hydraulic-fracturing-induced and natural earthquakes. The U.S. Geological Survey (USGS) generated one-year seismic hazard maps that accounted for both induced and natural earthquakes in the central and eastern U.S. from 2015 to 2018 (Petersen *et al.*, 2015, 2016, 2017, 2018). Wang *et al.* (2018) and Kothari and Shcherbakov (2019) used the ETAS model to describe earthquake occurrence induced by hydraulic fracturing in Alberta, Canada. However, there has been limited analysis on the hazard level in West Texas or the hazard for a shorter time range (i.e., during the days or weeks when operations are taking place near a particular site). Short-term hazard estimates are valuable because they vary greatly in time and space, and because hazard estimates could be used to make operational decisions to limit risks. Thus this project aims to develop a hazard assessment framework for West Texas that quantifies the regional hazard level over the injection period.

We also analyze the short-term hazard conditional on a given mainshock for wastewater disposal as well as natural earthquakes. The two types of induced earthquakes differ in various aspects (Ellsworth, 2013; Rubinstein and Mahani, 2015). Hydraulic fracturing lasts for hours to days with small injection volume (maximum of approximately 250,000 barrels), and the induced earthquakes tightly cluster around the injection wells. Wastewater disposal lasts for months to years and contains larger injection volume (usually 100,000 barrels/month or more), and thus affects a much wider region. Hydraulic-fracturing-induced earthquakes have smaller magnitudes (i.e., the maximum magnitude of 4.4 in Alberta, and possibly greater than 5.0 in Sichuan, China) compared to wastewater-disposal-induced earthquakes (i.e., magnitude of 5.8 in Oklahoma). As a result, the af-

tershock sequence of wastewater-disposal-induced earthquakes could be more important than that of hydraulic-fracturing-induced earthquakes, due to the larger magnitudes and higher contribution to the seismic hazard. These different features suggest that separate frameworks should be developed for these two types of induced seismicity.

Data and Processing

We considered three regions with seismicity dominated by differing phenomena: 1) hydraulic-fracturing-induced earthquakes in West Texas (Figure 1a), 2) wastewater-disposal-induced earthquakes in Oklahoma-Kansas (Figure 1b) and 3) natural earthquakes in California (Figure 1c). For the West Texas catalog, we obtained earthquake information from the TexNet. The magnitude of completeness (M_c) is 1.0, according to the Goodness of Fit test at the 90% level (Wiemer and Wyss, 2000). We collected all earthquakes occurring between 2018 and 2019 and with magnitudes greater than 1.5 and collected injection information for the same year from the FracFocus website (Figure 1a). For the Oklahoma-Kansas and California catalogs, M_c is 2.5 (Goodness of Fit test at 90% level) and 2.0 (Wiemer and Wyss, 2000), respectively. We collected a four-year catalog (2014-2018) for Oklahoma-Kansas and a 30-year catalog (1989-2019) for California with magnitudes greater than 2.7 from the USGS earthquake catalog website. The two catalogs were declustered using Reasenberg (1985). The three catalogs are summarized in Table 1. For every catalog, we used a more conservative magnitude cutoff instead of the estimated M_c.

Table 1: Summary of earthquake catalogs used for analysis.

	West Texas	**Oklahoma and Kansas**	**California**
$\boldsymbol{M_c}$	1.0	2.5	2.0
Date range	2018 - 2019	2014 - 2018	1989 - 2019
Area	$8 \times 10^3\ km^2$	$1.5 \times 10^5\ km^2$	$1.5 \times 10^5\ km^2$
Number of earthquakes	1,117	5,167	6,780

Hazard analysis for hydraulic-fracturing-induced earthquakes

Past research has observed that the hydraulic-fracturing-induced earthquakes tightly cluster around production wells in space and time (Atkinson *et al.*, 2016; Schultz *et al.*, 2018; Langenbruch *et al.*, 2018; Wang *et al.*, 2018). Thus the traditional short-term seismic occurrence model, Poissonian mainshocks with non-stationary aftershock sequences, is not sufficient to compute short-term hazard levels nearby an active hydraulic fracturing operation. Moreover, hydraulic-fracturing-induced earthquakes have small magnitudes, suggesting that their aftershocks should not have a significant contribution to the hazard level. Based on the above observations, we defined the short-term hazard level at a production site as the rate of exceeding a Modified Mercalli intensity (MMI) over the injection interval, given injection activity ($\lambda(MMI \geq x|injection)$). We used MMI as the intensity measure because $MMI = 3$ represents felt shaking. Hydraulic-fracturing-induced earthquakes rarely cause structural damage but can cause felt shaking and raise public concerns (Ellsworth, 2013).

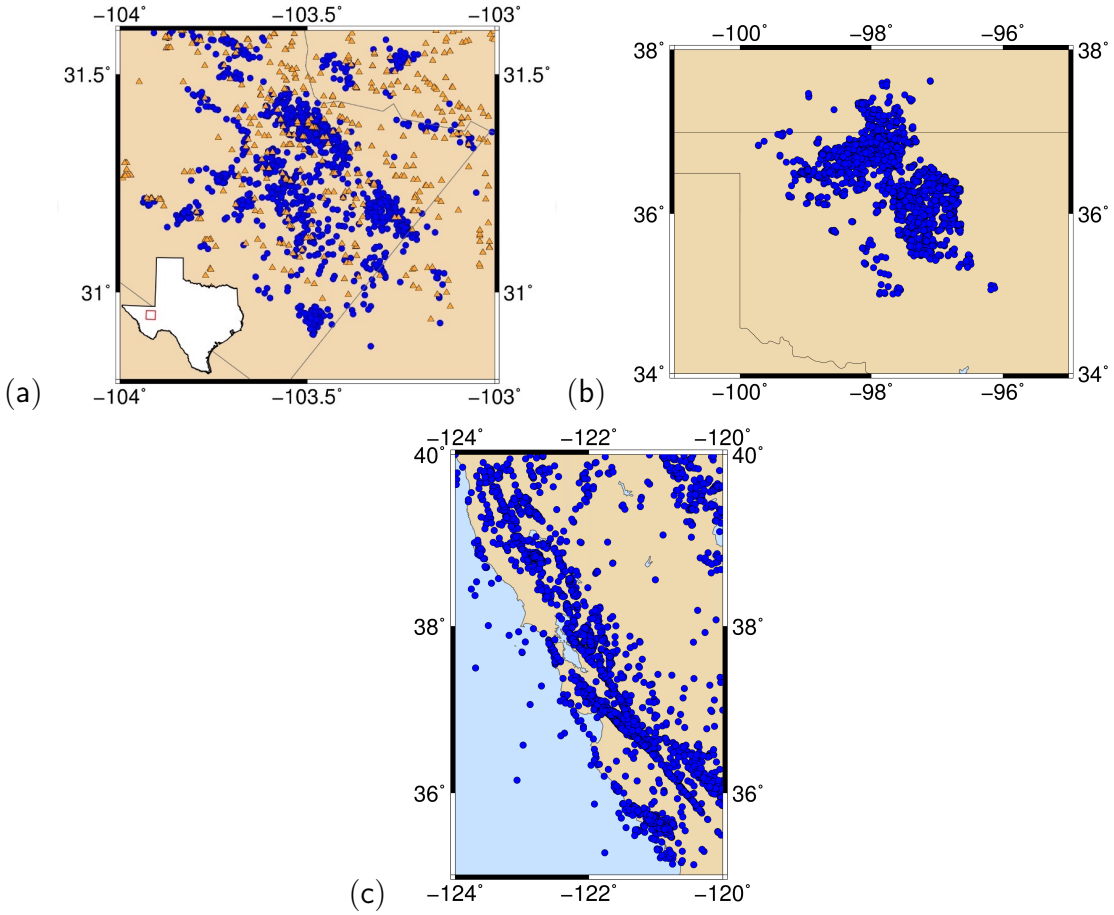

Figure 1: Earthquakes in (a) West Texas with $M \geq 1.5$, (b) Oklahoma and Kansas with $M \geq 2.7$ and (c) California with $M \geq 2.7$. Circles are earthquakes and triangles in West Texas are injection wells.

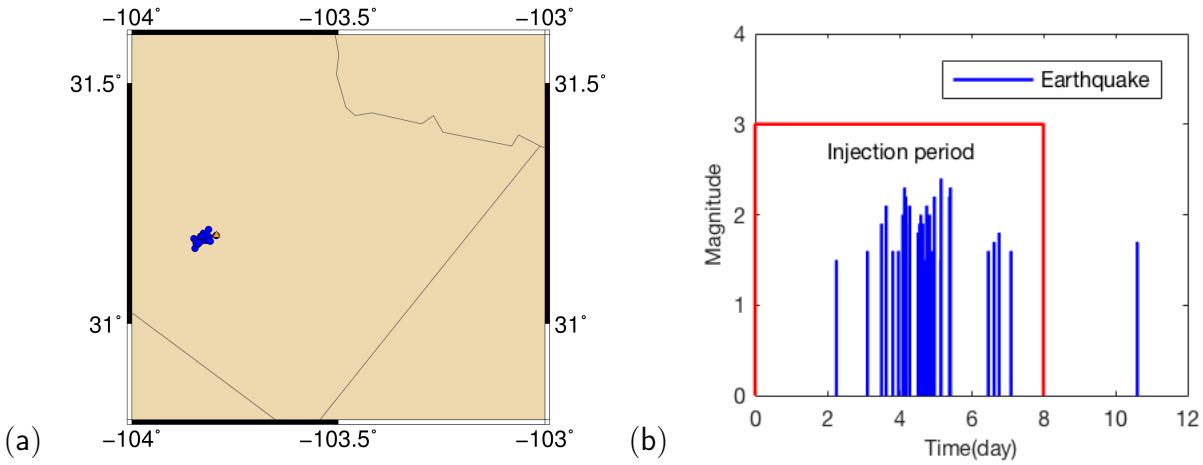

Figure 2: A cluster of earthquakes and the associated well. Their locations are shown in (a). The earthquake occurrence and the injection period are shown in (b).

Spatiotemporal Association Filter

Earthquakes were first associated with production wells based on a spatiotemporal association filter modified from Schultz *et al.* (2018): 1) the earthquake occurrence time should be during the injection period or within seven days of completion (hereafter referred to as the injection interval). 2) the earthquake epicenter should be within 6 km from the well surface location. We adjusted the Schultz *et al.* (2018) threshold from 5 km to 6 km due to the unknown trajectory length from the FracFocus website. Figure 2 shows an example earthquake cluster and its associated well. Most of the earthquakes happened within the injection interval and close to the site.

Effect of water injection volume

We first explored the relationship between a well's injection volume and its probability of inducing earthquakes. The spatiotemporal association filter method separated wells into seismogenic (i.e., wells that have associated earthquakes) and non-seismogenic wells. We conducted the Kolmogorov-Smirnov test (KS), the left-tailed Mann-Whitney U test (MN), and logistic regression to explore whether the seismogenic wells have significantly higher injection volumes than the non-seismogenic wells. The Kolmogorov-Smirnov test is used to check if two samples have the same probability distribution. The left-tailed Mann-Whitney U test is used to determine if the injection volume of seismogenic wells has a larger median than the injection volume of all wells. The logistic regression is used to describe the relationship between the dependent binary variable (i.e., seismogenic wells or not) and the independent variable (i.e., injection volume). The p-values of the Kolmogorov-Smirnov test and the Mann-Whitney U test at a significance level of 0.1 were 0.76 and 0.29, respectively (Figure 3a). Thus we were not able to reject the hypothesis that seismogenic wells are randomly sampled from the entire well distribution, nor to conclude that the median injection volume of seismogenic wells is larger than that of the parent distribution. The p-value of the logistic regression at a significance level of 0.05 was 0.05, and the McFadden pseudo R-squared was 0.005 (Figure 3b). Though the p-value could indicate some level of significance, the pseudo R-squared suggested a fit with large offsets. Figure 3b shows that most of the injection volumes are within a narrow range ($0.5 \times 10^5 m^3$ to $1 \times 10^5 m^3$), and the fitted curve is affected by the outliers below $1 \times 10^4 m^3$. Moreover, the probability stays around 0.5 for most of the data ($0.5 \times 10^5 m^3$ to $1 \times 10^5 m^3$). Thus

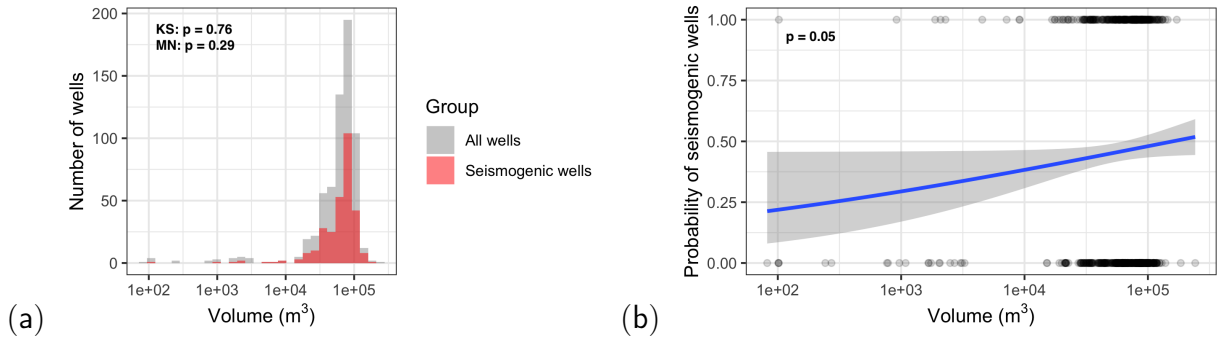

Figure 3: P-values of (a) the Kolmogorov-Smirnov test and the Mann-Whitney U test, and (b) logistic regression of seismogenic wells.

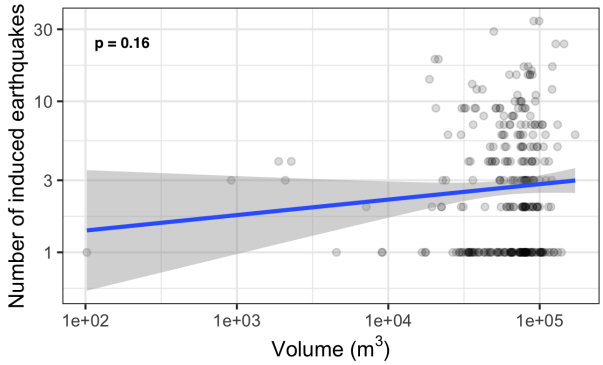

Figure 4: Linear regression of the number of induced earthquakes with respect to the injection volume.

we concluded that the relation between injection volume of a well and its probability of inducing earthquakes was not significant. We also performed linear regression analysis between the injection volume and the number of associated earthquakes (Figure 4), and found a p-value of 0.16 and $R^2 = 0.007$, suggesting a negligible linear relationship between the injection volume and the number of associated earthquakes.

We considered the situation where closely spaced injection wells could contribute to the pressure change at one location simultaneously. We then repeated the tests by grouping wells that were close in space (i.e., within 1km) and have overlapped injection periods into a single pad. Repeating the above analyses with these data produced similar statistical results, and the same conclusion was drawn. Though past studies have shown a monotonic relationship between the cumulative injection volume and the cumulative number of earthquakes for other regions (Schultz *et al.*, 2018; Langenbruch and Zoback, 2019; Shapiro *et al.*, 2010), when considering a short time window here (i.e., the injection period), the dependence of the number of earthquakes on the injection volume was negligible.

Hazard analysis framework

To estimate ground shaking hazard, we first predicted the number of earthquakes with magnitudes greater than M, induced during the injection interval using the following equation:

$$N(M_i \geq M|injection) = \delta_{HF} \cdot 10^a \cdot \frac{10^{-b(M-M_c)} - 10^{-b(M_{max}-M_c)}}{1 - 10^{-b(M_{max}-M_c)}} \quad (1)$$

where δ_{HF} is the probability that the injection well is seismogenic. Figure 5a shows the spatial distribution of $\hat{\delta}_{HF}$ for West Texas, showing that wells in the central region are more likely to induce earthquakes. 10^a is the number of earthquakes induced during the injection interval (Figure 5b). Both δ_{HF} and a were estimated using kriging, in order to characterize the spatial distribution of these parameter values based on observed data in the region. Detailed calculations are included in the electronic supplement. The last term describes a Gutenberg-Richter distribution truncated between M_c and M_{max}, where the spatial distribution of b-values was estimated using the method proposed by Kamer and Hiemer (2015). Figure 5c shows that b-values are smaller in the east region of the study area, where there were several earthquakes with magnitudes greater than 3.0. In this study, we considered magnitudes truncated between 1.5 and 6.0 (where the upper limit was chosen for convenience, as increasing or decreasing it by a unit does not affect the results below). The injection volume was excluded in the calculation according to the results in the previous section. However, Equation 1 could be easily modified to include such information for regions with a known relationship between injection volume and seismicity. Figure 6a shows the estimated number of earthquakes with magnitudes greater than 1.5 in West Texas, conditional on a nearby injection operation. The spatial distribution matches well with the observations (Figure 6b). We also conducted a prospective test using the 2019 catalog. Results showed that most of the recorded data were within the 95% confidence interval of the prediction. Detailed results are included in the electronic supplement.

We defined the short-term hazard at a production site as the rate of exceeding an MMI over the injection interval, given an injection. It was calculated by integrating over all possible magnitudes:

$$\lambda(MMI \geq x|injection) = \int_{M_c}^{M_{max}} P(MMI \geq x|m) \cdot N(M = m|injection) \cdot dm \quad (2)$$

$P(MMI \geq x|m)$ is the probability of exceeding an MMI given a magnitude m earthquake, calculated using the intensity prediction model (IPE) proposed by Atkinson *et al.* (2014). We assumed a constant hypocentral distance of $7.2km$ - the median distance between the induced earthquakes and the corresponding injection well. Using the same hypocentral distance for every earthquake has a minor influence on the hazard level because the IPE predicts relatively constant MMIs for distances within $10km$. The calculation could be easily adjusted to account for spatial variation of hypocentral distance. $N(M = m|injection)$ is the number of earthquakes with a magnitude of m during the injection interval, computed using Equation 1.

Figure 7 shows two hazard maps with different MMI thresholds. At $MMI = 3$ people start to feel the seismic shaking, and at $MMI = 5$ some non-structural damage occurs (Wood and Neumann, 1931). Figure 7 shows that the central and east parts of the study region have higher hazard levels for $MMI \geq 3$. For $MMI \geq 5$, negligible rates were estimated for the entire area except for the east region. This was due to the lower b-value in this area (Figure 5c). Figure 8 shows the locations of three example sites in the study region and their corresponding hazard curves. At small MMIs ($MMI \leq 3$), Site 2 has the highest hazard level, due to the high seismic productivity of wells (Figure 5b) and the substantial probability of seismogenic wells (Figure 5a) in that region.

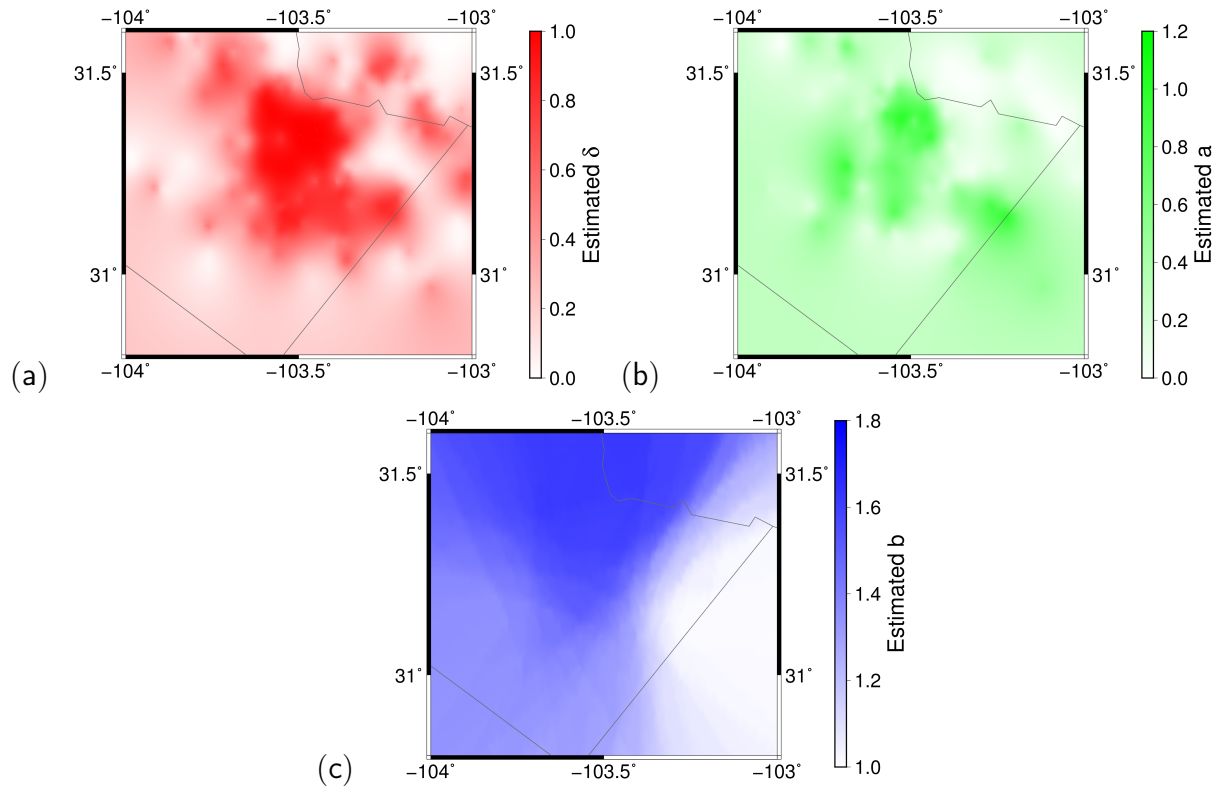

Figure 5: Estimated values of (a) δ_{HF} – the probability of a seismogenic well, (b) a – the seismic productivity of an injection well, and (c) b – the slope of the Gutenberg-Richter distribution.

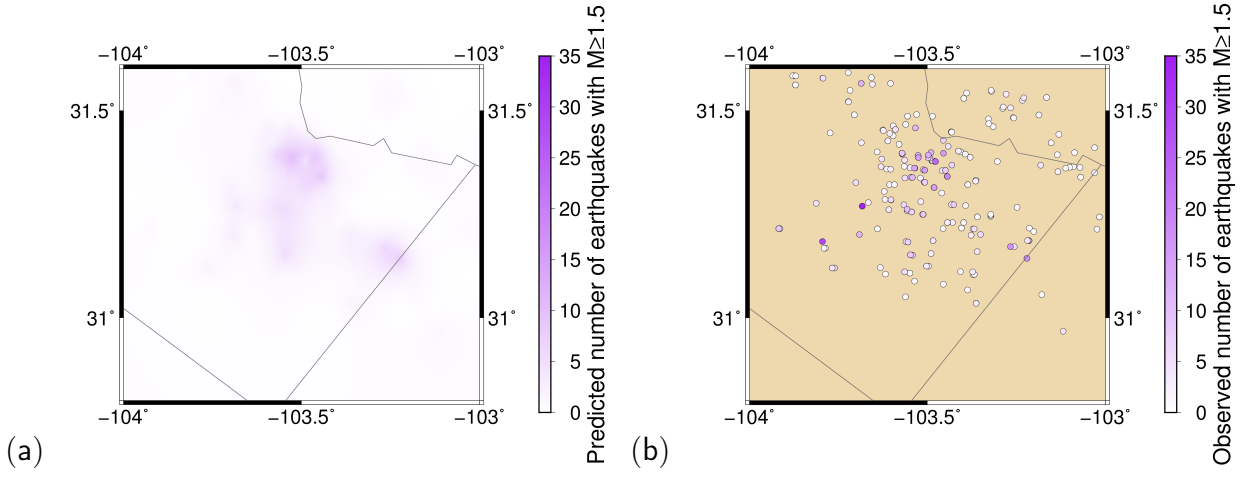

Figure 6: Number of induced earthquakes with $M \geq 1.5$ from (a) prediction and (b) observation.

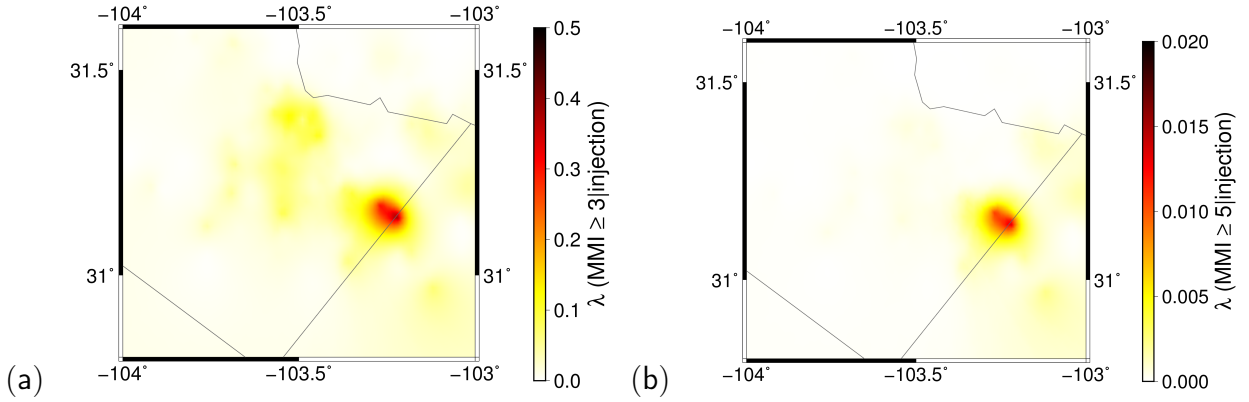

Figure 7: Rate of exceeding (a) $MMI \geq 3$ and (b) $MMI \geq 5$ given an injection during the injection interval. Unit: count per injection interval

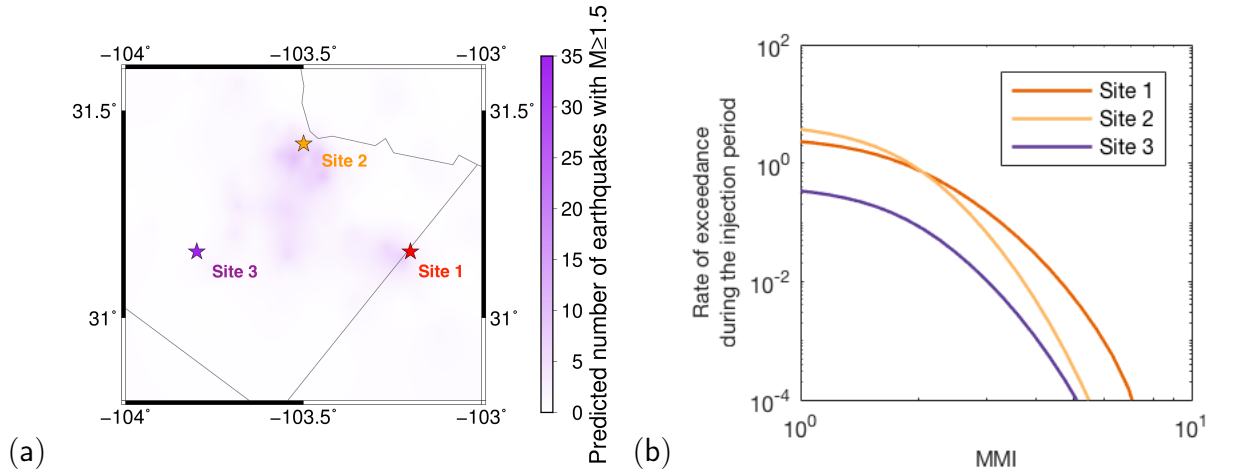

Figure 8: Hazard curves for three selected sites. The hazard is the rate of exceeding an MMI given an injection during the injection interval. (a) Locations of the sites. (b) MMI hazard curves for the sites.

Site 1 has the highest hazard level at larger MMIs because it has a lower b-value (Figure 5c). Site 3 has the lowest hazard level at all MMIs because it has the lowest seismic productivity of wells and the lowest probability of seismogenic wells. These observations agree well with the IPE hazard deaggregation, where earthquakes with $M < 3$ contribute over 40% of the hazard level for $MMI \geq 3$ but almost zero for $MMI \geq 5$. The details of hazard deaggregation are included in the electronic supplement.

From the analysis in this section, we see that the short-term hazard level is controlled by injection activities. Both b-values and the seismic productivity of injection wells are significant factors in the hazard analysis. Their relative importance varies with the ground motion amplitude level of interest (i.e., $MMI \leq 3$ versus $MMI \geq 3$).

Short-term hazard analysis for wastewater-disposal-induced and natural earthquakes

Hazard analysis for wastewater-disposal-induced earthquakes

Compared to hydraulic fracturing, wastewater disposal usually involves longer injection periods, larger injection volumes, and thus a wider affected region (Ellsworth, 2013; Rubinstein and Mahani, 2015). As a result, the seismic activity at one location could be associated with impacts from multiple disposal wells. Moreover, there is usually a time delay between the change of injection and the change of earthquake occurrence rate (Langenbruch and Zoback, 2016). Thus, compared to the hydraulic-fracturing-induced earthquakes, the spatial and temporal variation in the seismic hazard within a short time range is less significant. Moreover, wastewater-disposal-induced earthquakes have larger magnitudes and are capable of generating significant aftershock sequences (Ellsworth, 2013; Michael *et al.*, 2016). Therefore, we defined the short-term hazard level as the rate of exceeding an MMI over T days after a mainshock with a magnitude of M_m.

We assume that following the earthquake of magnitude M_m, there is a Poissonian mainshock rate of earthquakes plus a non-stationary aftershock sequence. The aftershock sequence was developed using the model of Reasenberg and Jones (1989). We estimated the earthquake rate with magnitudes greater than M, t days after an earthquake of M_m, using:

$$\lambda(M, t|M_m) = \lambda_M + \delta_{A|M_m} \cdot 10^{a+b(M_m-M)}(t+c)^{-p} \tag{3}$$

λ_M is the Poissonian mainshock rate computed using a truncated Gutenberg-Richter distribution between magnitudes 2.7 and 7.0, with $b = 1.16$ estimated from the 2016-2018 declustered catalog. The second half of the equation describes the aftershock sequence given a M_m mainshock. $\delta_{A|M_m}$ is the probability of the current earthquake triggering an aftershock sequence. We introduced $\delta_{A|M_m}$ to the original Reasenberg and Jones (1989) model because the aftershock parameters were estimated using sequences with aftershocks. Figure 9 shows the estimated values using logistic regression. Detailed calculation is included in the electronic supplement. The next term is the aftershock rate described in Reasenberg and Jones (1989), where c was 0.05, and b was 1.25 estimated from the aftershock catalog. The parameters $a = -1.62$ and $p = 0.78$ were computed from aftershock sequences in the catalog, using maximum likelihood estimation. In particular, we declustered the catalog using Reasenberg (1985) and estimated the parameters from aftershock sequences with at least five earthquakes. The median a and p were relatively stable when setting different thresholds of the number of aftershocks considered. This method was consistent with Reasenberg and Jones (1989), and we would compare the estimated parameters with the California generic parameters in Reasenberg and Jones (1989). Figure 10 shows the fitted aftershock sequences plotted against the average number of recorded earthquakes. The fit matches well with the observations for magnitudes between 3.0 and 5.5. Larger magnitudes were not plotted due to the limited sample size, and fit at smaller magnitudes was less important due to the low shaking intensity. The bias at smaller magnitudes is because of the limited number of aftershock sequences considered in the estimation. Only 13 out of 338 mainshocks with $3.0 \leq M \leq 4.0$ have at least five aftershocks, but the observed data in Figure 10 includes all aftershock sequences. Figure 10 also shows that the fitted line for $M \geq 5.0$ is slightly above the observed data due to observed aftershocks after eight days, which are not shown in the figure.

The hazard was defined as the rate of exceeding an MMI over T days after an observed earthquake

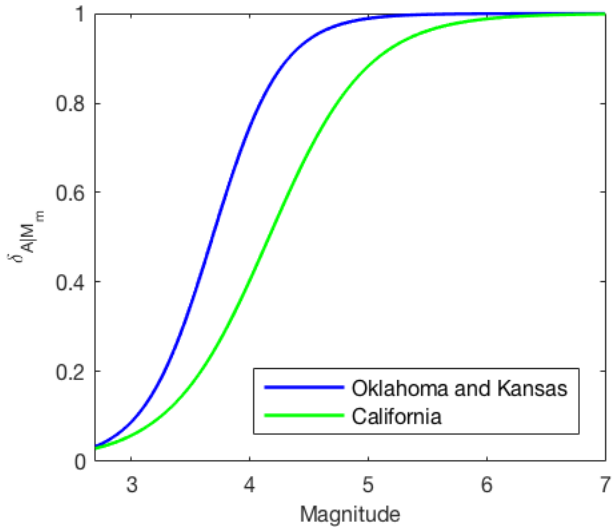

Figure 9: The probability of triggering aftershocks given an M_m mainshock ($\hat{\delta}_{A|M_m}$) for Oklahoma-Kansas and California.

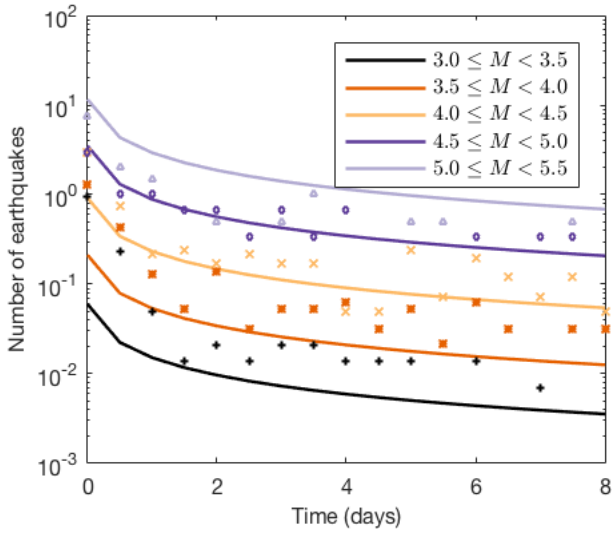

Figure 10: The fitted aftershock sequences plotted against the observed data. The lines are the fitted values, and dots are average numbers of earthquakes observed.

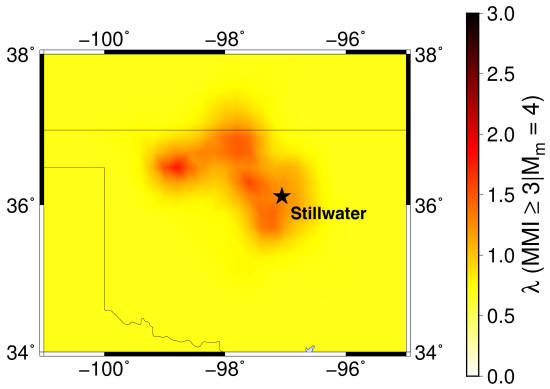

Figure 11: Rate of exceeding $MMI = 3$ over seven days after an $M_m = 4$ mainshock.

($M = M_m$). It was estimated using:

$$\lambda(MMI \geq x|M_m) = \int_0^T \int_{M_c}^{M_{max}} P(MMI \geq x|m) \cdot \lambda(m, t|M_m) \cdot dmdt \tag{4}$$

$P(MMI \geq x|m)$ is the probability of exceeding an MMI given a magnitude m earthquake, calculated from IPE proposed by Atkinson *et al.* (2014). For illustration, we assumed that the observed earthquake was $10km$ from the site of interest, and the average distance between its aftershocks and the site was also $10km$. $\lambda(m, t|M_m)$ is from Equation 3. T is the time range considered, and here was set to $7days$ for illustration. The region was divided into a $0.2^\circ \times 0.2^\circ$ grid, and a seismic source (with a seismic rate estimated from the declustered catalog) was located at the center of each grid.

Figure 11 shows the $MMI \geq 3$ hazard map conditional on a magnitude 4.0 mainshock, with the above assumptions. It shows that regions without recorded earthquakes have constant hazard levels, which is the hazard from aftershock sequences of the assumed mainshock. The aftershock hazard is constant because of the same aftershock parameters are used statewide. Mainshocks in these areas will be extremely rare, but conditional upon their occurrence, there would be short-term aftershock hazard. Central Oklahoma has a much higher hazard (for this low-amplitude shaking level) due to the high Poissonian mainshock rate of earthquakes in this region. We plotted hazard curves for Stillwater conditional on three mainshock magnitude (M_m) values (Figure 12). Overall, the larger the observed magnitude, the higher the hazard level, because the aftershock sequence is stronger for a larger mainshock.

More recent studies have modified and updated the Reasenberg and Jones (1989) aftershock model and parameters. Page *et al.* (2016) considered earthquakes with $M > 6$ and developed regional aftershock parameters for tectonic regions in Garcia *et al.* (2012). They identified the aftershocks using window methods and included sequences with few or no aftershocks in their calculation. As a result, they found a much smaller a-value compared to Reasenberg and Jones (1989). They also modified the Reasenberg and Jones (1989) aftershock model by considering the temporal variation of the magnitude of completeness and the parameter uncertainty. The generic parameters and modified model were then implemented and updated by Hardebeck *et al.* (2019) for California, Michael *et al.* (2016) for the M5.8 Pawnee, Oklahoma, earthquake and Michael *et al.* (2020) for the M7.1 earthquake at Anchorage, Alaska. The works mentioned above are based on aftershock sequences of large mainshocks (i.e., $M > 5$), whereas most earthquakes in Oklahoma have relatively small magnitudes. Our parameters were developed based on smaller earthquakes

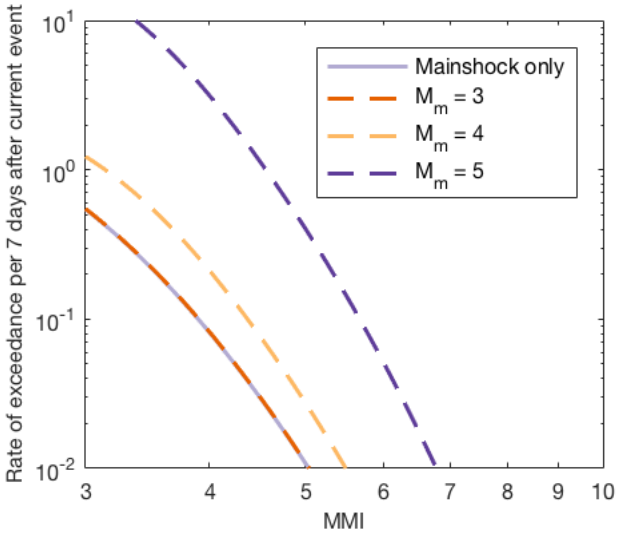

Figure 12: Seven-day hazard curves for Stillwater, conditional on three mainshock magnitude (M_m) values. The hazard is the rate of exceeding an MMI over seven days after an M_m mainshock.

and were declustering algorithm dependent. Our estimated a-value was much larger than Page *et al.* (2016) and Michael *et al.* (2016). Some possible reasons could be: 1) we only considered sequences with at least five aftershocks; 2) the majority of mainshocks we considered were smaller earthquakes with $M < 5$; 3) the declustering algorithm may include secondary aftershock sequences. If only considering mainshocks with $M > 5$, we resulted in $a = -2.59$, similar to the values in Page *et al.* (2016) and Michael *et al.* (2016). The proposed model could be modified with different parameter values to capture parameter uncertainties. We repeated hazard analysis using the parameters developed by Page *et al.* (2016) (included in the electronic supplement). Though the hazard levels from the two sets of parameters differ, both suggest that the Poissonian mainshocks contribute substantially to the short-term hazard level in central Oklahoma.

Comparison between Oklahoma-Kansas and California

We repeated the hazard analysis for California using Equation 4, to explore the difference between hazard from natural and wastewater-disposal-induced earthquakes. For California, we used the generic parameters in Reasenberg and Jones (1989) to estimate the aftershock rate, and a truncated Gutenberg-Richter distribution between 2.7 and 9.0, with $b = 1.0$, to estimate to estimate the Poissonian mainshock rate. Table 2 summarizes the aftershock parameters for Oklahoma-Kansas and California. Compared to the California catalog, the Oklahoma-Kansas catalog had a larger a-value, suggesting higher aftershock productivity, and a smaller p-value, suggesting a slower decay in aftershock rate. The high aftershock productivity in Oklahoma was also observed in Michael *et al.* (2016),Llenos and Michael (2013), and Goebel *et al.* (2019).

In addition to aftershock parameters, the two regions also differ significantly in the probability of triggering aftershocks. Figure 9 shows that for a given magnitude, mainshocks in Oklahoma-Kansas is more likely to trigger aftershocks. The difference became significant for magnitudes around 4.5. This could be partly explained by secondary aftershock sequences. In California, many earthquakes with magnitudes between 4.0 and 4.5 were aftershocks of larger mainshocks. As a result, the magnitude 4.5 earthquake, together with its aftershocks, were declustered and excluded

Table 2: Aftershock parameters.

	California	**Oklahoma-Kansas**
$\boldsymbol{a}$	-1.76	-1.62
$\boldsymbol{p}$	1.07	0.78
$\boldsymbol{c}$	0.05	0.05
$\boldsymbol{b}$	0.90	1.25

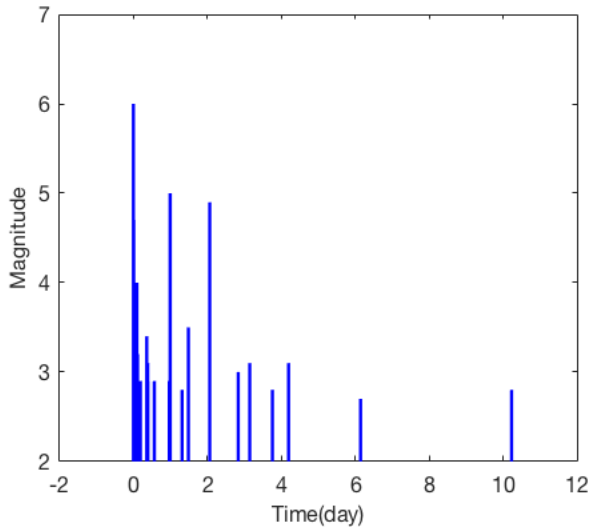

Figure 13: A cluster of earthquakes with a $M_m = 6$ mainshock.

in the estimation. Figure 13 shows an earthquake cluster with an M6 mainshock in California. The M4 earthquake, and its aftershock sequence, were considered as aftershocks of the M6 mainshock by the declustering algorithm. For California, 31% of the earthquakes with magnitudes between 4.0 and 4.5 were aftershocks of larger mainshocks, whereas, for the Oklahoma and Kansas region, the percentage was 20%.

We generated hazard curves for San Francisco and Stillwater and computed the aftershock contribution for these two cities. The aftershock contribution was the ratio between two $\lambda(MMI \geq x|M_m)$ values, where one was computed considering only aftershocks sequences, and one was computed considering both aftershocks and Poissonian mainshocks using Equations 3 and 4. Figure 14 summarizes the contribution from aftershocks for three mainshock magnitude (M_m) values. It shows that the larger the mainshock, the higher the contribution from aftershocks. Moreover, for all magnitudes and MMIs, aftershocks in San Francisco have a larger contribution compared to Stillwater. In conclusion, for regions with natural earthquakes, the aftershock sequences contribute significantly to the short-term seismic hazard, whereas for wastewater-disposal-induced earthquakes, the Poissonian mainshock rate could be critical.

Discussion

By comparing the hazard analysis in West Texas, Oklahoma-Kansas, and California, we concluded that for different regions, factors that affect the short-term seismic hazard differ significantly. The

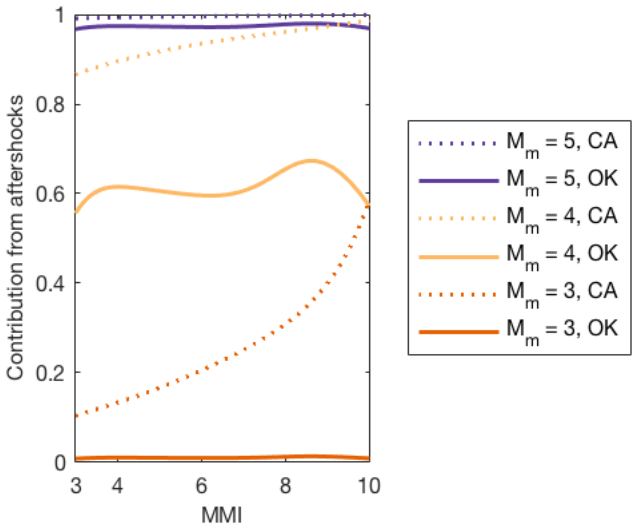

Figure 14: Aftershock contribution to short-term hazard levels for Stillwater in Oklahoma (OK) and San Francisco in California (CA).

observations are briefly summarized in Table 3. For hydraulic-fracturing-induced earthquakes in West Texas, earthquakes induced by injection activities cluster closely around the wells in time and space. Thus the hazard during the injection interval has large temporal and spatial variations. To better capture such variation, we quantified the short-term hazard considering the injection information, as well as regional seismic features. We concluded that clustered earthquakes dominate the hazard. Thus injection activities are the driver of the short-term hazard at the production site.

Table 3: Significance of different factors on the short-term hazard level

	West Texas	**Oklahoma and Kansas**	**California**
Mainshocks	Negligible	More significant	Significant
Aftershocks	Negligible	Significant	More significant
Clustered earthquakes	Large	Negligible	Negligible

In Oklahoma-Kansas, disposal activities usually involve a wider area and a longer time, with no short-term linkage between water disposal on the earthquake occurrence. As a result, we defined the short-term hazard level as the rate of exceeding an MMI over T days after an observed earthquake with a magnitude of M_m and used a Poissonian mainshock and non-stationary aftershock model to describe the short-term occurrence. We used this model to conduct hazard analyses for both Stillwater in Oklahoma-Kansas and San Francisco in California. Though the same hazard model was implemented, the two cities differed in terms of the hazard deaggregation - aftershocks in San Francisco always had more substantial hazard contributions compared to those in Stillwater. For wastewater-disposal-induced earthquakes, the Poissonian mainshock rate could contribute significantly to the short-term seismic hazard (Figure 11). However, the difference would become negligible if the mainshock rate in Oklahoma-Kansas declines. This emphasizes that for wastewater-disposal-induced earthquakes, though no injection information was involved in the short-term hazard calculation, the resulted hazard level could be affected by the mainshock rate, which was controlled

by injection activities.

Conclusion

This study conducted short-term hazard analysis for regions with induced seismicity, with a focus on hydraulic-fracturing-induced earthquakes in West Texas and wastewater-disposal-induced earthquakes in Oklahoma-Kansas. We also compared the results to those in California.

Hydraulic-fracturing-induced earthquakes tightly cluster around injection activities, which results in a large spatial and temporal variation in hazard levels. We developed a framework to estimate the short-term hazard level at the production site, defined as the rate of exceeding an MMI over the injection interval, given an injection. Our model considered injection information, as well as regional seismic features. We found that the injection volume had a negligible effect on the induced seismic rate due to the short time window considered. However, the framework could be easily modified to include such information for other regions with a known relationship between injection volume and seismicity. Results suggested that the seismic productivity of injection wells and b-values are important factors in the hazard analysis. For smaller MMI thresholds (i.e., $MMI < 3$), regions with more seismogenic wells had considerable hazard levels. However, for larger MMI thresholds (i.e., $MMI > 5$), regions with smaller b-values had higher hazard levels compared to the rest of the area. This suggests that different factors should be considered for different target performances. We conclude that earthquakes clustered around the injection wells dominate the short-term hazard level at production sites. Thus injection activities are the drivers of the short-term hazard for hydraulic-fracturing-induced earthquakes.

For both wastewater-disposal-induced and natural earthquakes, the hazard level was defined as the rate of exceeding an MMI over T days after an observed earthquake with a magnitude of M_m. We used Poissonian mainshock rates with non-stationary aftershocks to describe the short-term earthquake occurrence and performed hazard analysis for Stillwater and San Francisco. We observed that, given the same magnitude, earthquakes in Oklahoma-Kansas were more likely to trigger aftershocks compared to those in California. The difference was most significant for magnitudes around 4.5. This was due to the presence of secondary aftershock sequences in the California catalog. Comparing hazard curves for Stillwater and San Francisco, we observed that aftershocks in San Francisco always had a higher contribution compared to those in Stillwater. For Oklahoma-Kansas, the mainshock rate contributed significantly to the short-term hazard level, especially for small-moderate mainshocks. Areas with observed induced earthquakes had much higher hazard levels than the rest of the region. This suggests that for wastewater-disposal-induced earthquakes, though no injection information was included in the short-term hazard calculation, the resulted hazard level could be affected by the mainshock rate.

Data and Resources

The earthquake occurrences in California and the Oklahoma and Kansas region were obtained from the USGS earthquake catalog website (https://earthquake.usgs.gov/earthquakes/search, last accessed September 2019). The earthquake catalog for West Texas was obtained from TexNet (https://www.beg.utexas.edu/texnet-cisr/texnet/earthquake-catalog, last accessed January 2020). The hydraulic fracturing information for West Texas was obtained from FracFocus (https://fracfocus.org/, last accessed January 2020). Detailed calculations are included in the electronic supplement.

Acknowledgement

We thank William Ellsworth, Anne Kiremidjian, Ryan Schultz, and Andrew Michael for their helpful feedback. Funding for this work came from the Stanford Center for Induced and Triggered Seismicity.

References

Agnew, D. C., and L. M. Jones (1991). Prediction probabilities from foreshocks, *Journal of Geophysical Research: Solid Earth* **96**(B7), 11959–11971.

Atkinson, G. M., D. W. Eaton, H. Ghofrani, D. Walker, B. Cheadle, R. Schultz, R. Shcherbakov, K. Tiampo, J. Gu, R. M. Harrington, *et al.* (2016). Hydraulic fracturing and seismicity in the western canada sedimentary basin, *Seismological research letters* **87**(3), 631–647.

Atkinson, G. M., C. B. Worden, and D. J. Wald (2014). Intensity prediction equations for north america, *Bulletin of the Seismological Society of America* **104**(6), 3084–3093.

Ellsworth, W. L. (2013). Injection-induced earthquakes, *Science* **341**(6142), 1225942.

Field, E. H., K. R. Milner, J. L. Hardebeck, M. T. Page, N. van der Elst, T. H. Jordan, A. J. Michael, B. E. Shaw, and M. J. Werner (2017). A spatiotemporal clustering model for the third uniform california earthquake rupture forecast (ucerf3-etas): Toward an operational earthquake forecast, *Bulletin of the Seismological Society of America* **107**(3), 1049–1081.

Frohlich, C., H. DeShon, B. Stump, C. Hayward, M. Hornbach, and J. I. Walter (2016). A historical review of induced earthquakes in texas, *Seismological Research Letters* **87**(4), 1022–1038.

Garcia, D., D. J. Wald, and M. Hearne (2012). A global earthquake discrimination scheme to optimize ground-motion prediction equation selection, *Bulletin of the Seismological Society of America* **102**(1), 185–203.

Gerstenberger, M. C., S. Wiemer, L. M. Jones, and P. A. Reasenberg (2005). Real-time forecasts of tomorrow's earthquakes in california, *Nature* **435**(7040), 328.

Ghofrani, H., G. M. Atkinson, R. Schultz, and K. Assatourians (2019). Short-term hindcasts of seismic hazard in the western canada sedimentary basin caused by induced and natural earthquakes, *Seismological Research Letters* **90**(3), 1420–1435.

Goebel, T., Z. Rosson, E. Brodsky, and J. Walter (2019). Aftershock deficiency of induced earthquake sequences during rapid mitigation efforts in oklahoma, *Earth and Planetary Science Letters* **522**, 135–143.

Hardebeck, J. L., A. L. Llenos, A. J. Michael, M. T. Page, and N. Van Der Elst (2019). Updated california aftershock parameters, *Seismological Research Letters* **90**(1), 262–270.

Kamer, Y., and S. Hiemer (2015). Data-driven spatial b value estimation with applications to california seismicity: To b or not to b, *Journal of Geophysical Research: Solid Earth* **120**(7), 5191–5214.

Kothari, S., and R. Shcherbakov (2019). Statistical modelling and characterization of induced seismicity across the western canada sedimentary basin, in *AGU Fall Meeting 2019*, AGU.

Langenbruch, C., M. Weingarten, and M. D. Zoback (2018). Physics-based forecasting of man-made earthquake hazards in oklahoma and kansas, *Nature communications* **9**(1), 3946.

Langenbruch, C., and M. D. Zoback (2016). How will induced seismicity in oklahoma respond to decreased saltwater injection rates?, *Science advances* **2**(11), e1601542.

Langenbruch, C., and M. D. Zoback (2019). Assessing and managing seismic hazards in oklahoma associated with hydraulic fracturing, in *AGU Fall Meeting 2019*, AGU.

Llenos, A. L., and A. J. Michael (2013). Modeling earthquake rate changes in oklahoma and arkansas: Possible signatures of induced seismicity, *Bulletin of the Seismological Society of America* **103**(5), 2850–2861.

Michael, A., E. Field, J. Hardebeck, A. Llenos, K. Milner, M. Page, S. Perry, N. van der Elst, and A. Wein (2016). Aftershock forecasting: Recent developments and lessons from the 2016 m5. 8 pawnee, oklahoma, earthquake, in *AGU Fall Meeting Abstracts*.

Michael, A. J. (2012). Fundamental questions of earthquake statistics, source behavior, and the estimation of earthquake probabilities from possible foreshocks, *Bulletin of the Seismological Society of America* **102**(6), 2547–2562.

Michael, A. J., S. K. McBride, J. L. Hardebeck, M. Barall, E. Martinez, M. T. Page, N. van der Elst, E. H. Field, K. R. Milner, and A. M. Wein (2020). Statistical seismology and communication of the usgs operational aftershock forecasts for the 30 november 2018 m w 7.1 anchorage, alaska, earthquake, *Seismological Research Letters* **91**(1), 153–173.

Page, M. T., N. Van Der Elst, J. Hardebeck, K. Felzer, and A. J. Michael (2016). Three ingredients for improved global aftershock forecasts: Tectonic region, time-dependent catalog incompleteness, and intersequence variability, *Bulletin of the Seismological Society of America* **106**(5), 2290–2301.

Petersen, M. D., C. S. Mueller, M. P. Moschetti, S. M. Hoover, A. L. Llenos, W. L. Ellsworth, A. J. Michael, J. L. Rubinstein, A. F. McGarr, and K. S. Rukstales (2016). Seismic-hazard forecast for 2016 including induced and natural earthquakes in the central and eastern united states, *Seismological Research Letters* **87**(6), 1327–1341.

Petersen, M. D., C. S. Mueller, M. P. Moschetti, S. M. Hoover, J. L. Rubinstein, A. L. Llenos, A. J. Michael, W. L. Ellsworth, A. F. McGarr, A. A. Holland, *et al.* (2015). Incorporating induced seismicity in the 2014 united states national seismic hazard model: Results of 2014 workshop and sensitivity studies .

Petersen, M. D., C. S. Mueller, M. P. Moschetti, S. M. Hoover, K. S. Rukstales, D. E. McNamara, R. A. Williams, A. M. Shumway, P. M. Powers, P. S. Earle, *et al.* (2018). 2018 one-year seismic hazard forecast for the central and eastern united states from induced and natural earthquakes, *Seismological Research Letters* **89**(3), 1049–1061.

Petersen, M. D., C. S. Mueller, M. P. Moschetti, S. M. Hoover, A. M. Shumway, D. E. McNamara, R. A. Williams, A. L. Llenos, W. L. Ellsworth, A. J. Michael, *et al.* (2017). 2017 one-year seismic-hazard forecast for the central and eastern united states from induced and natural earthquakes, *Seismological Research Letters* **88**(3), 772–783.

Reasenberg, P. (1985). Second-order moment of central california seismicity, 1969–1982, *Journal of Geophysical Research: Solid Earth* **90**(B7), 5479–5495.

Reasenberg, P. A., and L. M. Jones (1989). Earthquake hazard after a mainshock in california, *Science* **243**(4895), 1173–1176.

Rubinstein, J. L., and A. B. Mahani (2015). Myths and facts on wastewater injection, hydraulic fracturing, enhanced oil recovery, and induced seismicity, *Seismological Research Letters* **86**(4), 1060–1067.

Schultz, R., G. Atkinson, D. Eaton, Y. Gu, and H. Kao (2018). Hydraulic fracturing volume is associated with induced earthquake productivity in the duvernay play, *Science* **359**(6373), 304–308.

Shapiro, S. A., C. Dinske, C. Langenbruch, and F. Wenzel (2010). Seismogenic index and magnitude probability of earthquakes induced during reservoir fluid stimulations, *The Leading Edge* **29**(3), 304–309.

Snee, J.-E. L., and M. D. Zoback (2018). State of stress in the permian basin, texas and new mexico: Implications for induced seismicity, *The Leading Edge* **37**(2), 127–134.

Wang, R., R. Shcherbakov, G. M. Atkinson, and K. Assatourians (2018). Stochastic simulation of hydraulic fracturing induced seismicity: case studies in alberta, canada, in *AGU Fall Meeting Abstracts*.

Wiemer, S., and M. Wyss (2000). Minimum magnitude of completeness in earthquake catalogs: Examples from alaska, the western united states, and japan, *Bulletin of the Seismological Society of America* **90**(4), 859–869.

Wood, H. O., and F. Neumann (1931). Modified mercalli intensity scale of 1931, *Bulletin of the Seismological Society of America* **21**(4), 277–283.